Intersecting topological nodal ring and nodal wall states in superhard superconductor FeB_4

Feng Zhou,[1] Ying Liu,[2,*] Jianhua Wang,[1] Minquan Kuang,[1] Tie Yang,[1] Hong Chen,[1] Xiaotian Wang,[1,†] and Zhenxiang Cheng[3,‡]

[1]*School of Physical Science and Technology, Southwest University, Chongqing 400715, China*
[2]*School of Materials Science and Engineering, Hebei University of Technology, Tianjin 300130, China*
[3]*Institute for Superconducting and Electronic Materials (ISEM), University of Wollongong, Wollongong 2500, Australia*

(Received 2 January 2021; accepted 19 July 2021; published 29 July 2021)

Novel materials with both topological nontrivial states and superconductivity have attracted considerable attention in recent years. Single-crystal FeB_4 was recently synthesized and demonstrated to exhibit superconductivity at temperatures lower than 2.9 K, and its nanoindentation hardness was measured to be 65 GPa. In this study, based on first-principles calculations and the low-energy $\boldsymbol{k \cdot p}$ effective Hamiltonian, we found that this *Pnnm*-type superhard FeB_4 superconductor hosts topological behaviors with intersecting nodal rings (INRs) in the $k_x = 0$ and $k_z = 0$ planes and nodal wall states in the $k_y = \pi$ and $k_z = \pi$ planes. The observed surface drum-head-like (D-H-L) states on the [100] and [001] surfaces confirmed the presence of INR states in this system. According to our investigation results, FeB_4, with its superconductivity, superior mechanical behaviors, one-dimensional and two-dimensional topological elements, and D-H-L surface states, is an existing single-phase target material that can be used to realize the topological superconducting state in the near future.

DOI: 10.1103/PhysRevMaterials.5.074201

I. INTRODUCTION

Topological superconductors (TSCs) [1–5] can be used to achieve Majorana bound states and other exotic physical properties, for example, emergent supersymmetry. Therefore, in recent years, the quest to design and search for new TSCs has emerged as one of the most important directions in condensed matter physics and quantum chemistry. In general, two approaches are followed to design topological superconductors. The first approach [6] involves constructing heterostructures consisting of topological materials (TMs) and superconducting materials (SCMs), followed by use of the proximity effect to achieve topological superconductivity. In this approach, one should consider the lattice mismatch and interface reactions between the two materials, which usually hinder successful construction of the heterostructure. The second approach [1,7–10] involves achieving topological superconductivity in a single-phase material instead of a heterostructure. In this approach, one can select an SCM or a TM as the starting material platform and subsequently induce the topological property or superconductivity in the said material.

To date, a few topological insulators and topological semimetals that feature nodal points and superconductivity have been reported. For example, Bi_2Se_3 [11] is a well-known topological insulator, and Hor *et al.* [12] reported that Cu intercalation in the gaps between two Bi_2Se_3 layers can induce superconductivity at 3.8 K in $Cu_xBi_2Se_3$, where $x =$ 0.12-0.15. Similarly, in 2015, Liu *et al.* [13] reported the existence of superconducting and surface topological states in $Sr_{0.065}Bi_2Se_3$. In Cd_3As_2 [14] and tungsten ditelluride [15] materials with a zero-dimensional (0D) topological element (TE), superconductivity can be induced by applying high pressure. Furthermore, $MoTe_2$ [16], a sister compound of tungsten ditelluride, was proved to exhibit the Weyl semimetallic property and to intrinsically host superconductivity with a transition temperature (T_c) of 0.10 K. In 2019, based on first-principles calculations, Song *et al.* [17] predicted that highly stable two-dimensional (2D) rect-AlB_6 material features triple Dirac cones, a remarkable motif, and possibly an intrinsic superconducting character.

Recently, researchers have also been keen to develop materials that feature both topological nodal lines (NLs) and superconducting states. Thus far, a handful of known TMs with a one-dimensional (1D) TE accompanied by superconductivity have been predicted, including NaAlSi [18], [Ti/Mg]Bi_2 [19,20], [Sn/Pb]$TaSe_2$ [21,22], $SrAs_3$ [23,24], and In_xTaS_2 [25]. To the best of our knowledge, TMs with a 2D TE, namely, nodal wall (also called nodal surface) [26–28] states and possible superconductivity, have not been analyzed by researchers. Therefore the search for highly stable, purpose-built TMs with simultaneous 1D/2D TE and superconducting states is highly significant.

In the present work, we study the topological property of a superhard iron tetraboride superconductor, namely, FeB_4, with the *Pnnm*-type structure [29]. Gou *et al.* [29] synthesized single crystals of *Pnnm*-type FeB_4 at pressures higher than 8 GPa and high temperatures. Interestingly, this system [29] has been proved to exhibit bulk superconductivity at temperatures lower than 2.9 K based on magnetic susceptibility measurements. Moreover, FeB_4 has high levels of hardness, that is, no phase transitions occur at ambient temperature in a

*ying_liu@hebut.edu.cn
†xiaotianwang@swu.edu.cn
‡cheng@uow.edu.au

 ©2021 American Physical Society

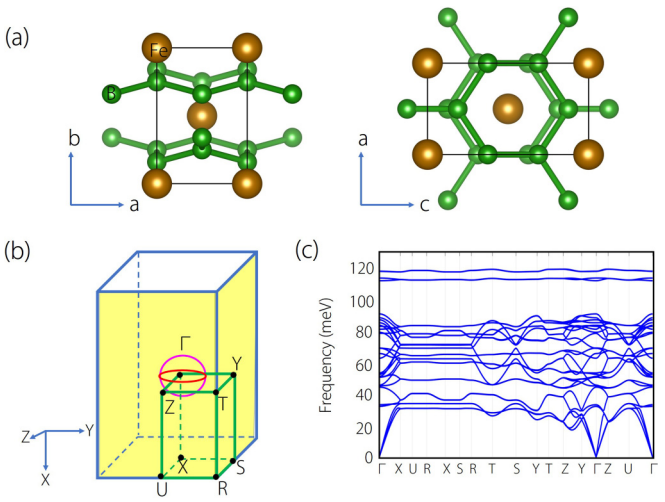

FIG. 1. (a) Crystal structures of *Pnnm*-type FeB_4 system from different views; the green and brown spheres represent B and Fe atoms, respectively; (b) bulk Brillouin zone (BZ) and the schematic diagram of NR and nodal wall states; and (c) calculated phonon dispersion of the FeB_4 system along the Γ-X-U-R-X-S-R-T-S-Y-T-Z-Y-Γ-Z-U-Γ paths.

diamond anvil cell under pressures of up to ca. 40 GPa. Hence, this superhard FeB_4 superconductor can be viewed as an excellent target material to study the perfect mechanical and superconductivity properties [29]. Based on first-principles calculations, we reveal that this prepared compound is also a topological material with 1D nodal rings (NRs) and 2D nodal walls. Importantly, our work is for the first time to report a superconductor co-hosts 1D and 2D topological elements. Therefore FeB_4 is likely to be a suitable material for achieving topological superconductivity.

II. MATERIASLS AND COMPUTATIONAL METHODS

The band structures and topological signatures were obtained using the VASP code [30]. The exchange-correlation potential was treated using the generalized gradient approximation (GGA) [31] with the Perdew-Burke-Ernzerhof (PBE) [32] functional. The cutoff energy was set to 600 eV. A Monkhorst-Pack special 11 × 7 × 7 k-point mesh was used in the BZ integration. The surface states of FeB_4, including the [100] and [001] surface states, were investigated using the WANNIERTOOLS software application [33]. The phonon dispersion of FeB_4 was calculated using the NANODCAL code [34] and the force-constants method.

The optimized crystal structures of *Pnnm* FeB_4 are shown in Fig. 1(a), where the Fe atoms and B atoms occupy the 2a, and 4g Wyckoff positions, respectively. The optimized lattice constants are $a = 3.00$ Å, $b = 4.503$ Å, and $c = 5.278$ Å. The obtained values are close to the experimental data of FeB_4 [29] ($a = 2.99$ Å, $b = 4.578$ Å, and $c = 5.298$ Å). The phonon dispersion of the FeB_4 system along the Γ-X-U-R-X-S-R-T-S-Y-T-Z-Y-Γ-Z-U-Γ paths [see Fig. 1(b)] is shown in Fig. 1(c). The lack of imaginary frequencies in the phonon dispersion indicates the dynamic stability of this system.

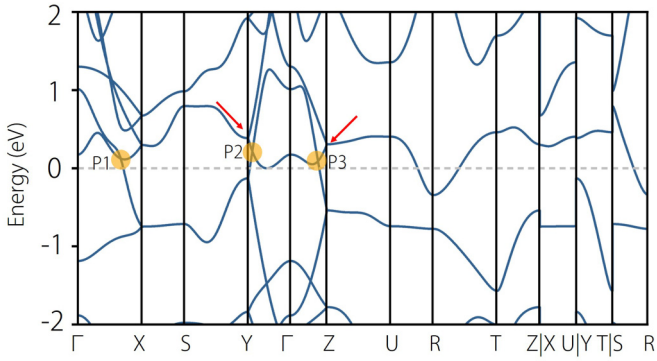

FIG. 2. Band structure of FeB_4 along the Γ-X-S-Y-Γ-Z-U-R-T-Z|X-U|Y-T|S-R paths. The BCPs around the Fermi level are labeled P1, P2, and P3.

III. INTERSECTING NODAL RING AND NODAL WALL STATES

Figure 2 shows the band structure of FeB_4 without the spin-orbit coupling (SOC). FeB_4 is a metallic system with three clear band-crossing points (BCPs) [35,36], one each along the Γ-X, Y-Γ, and Γ-Z paths, named P1, P2, and P3, respectively. Given that Fe is a transition metal, the DFT + U calculation [37,38], where U is the Hubbard correction, was performed to examine its electronic structures (see Fig. S1 in Ref. [39]). In Fig. S1 [39], one can see three clear BCPs around the Fermi level (E_F) that persist when U = 2-5 eV. Because FeB_4 has $\mathcal{P}$ and time-reversal $\mathcal{T}$ symmetries, points P1, P2, and P3 should not be isolated, as argued by Weng *et al.* [40–43]. To confirm the nodal states of the FeB_4 system, we performed a detailed scan of the band structures along the selected k-paths in the $k_{(x,y,z)} = 0$ planes [see Figs. 3(a), 4(a), and 5(a)].

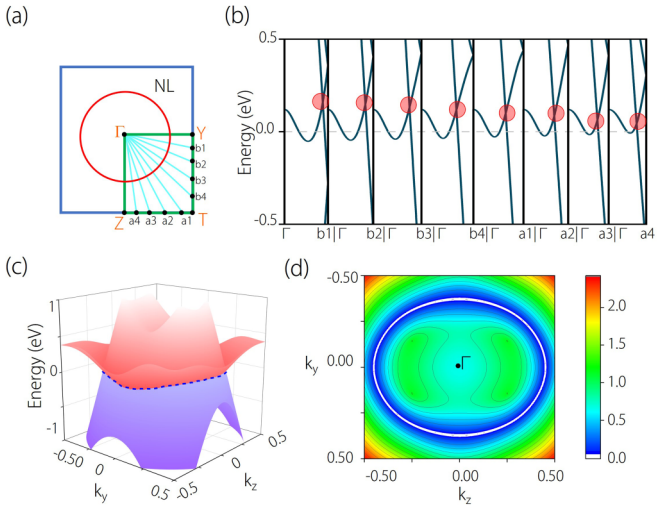

FIG. 3. (a) Selected k paths on the $k_x = 0$ plane. The points a1–a4 (b1–b4) are equally spaced between T and Z (Y and T); (b) the band structures of the Γ-a1/a2/a3/a4 and Γ-b1/b2/b3/b4 paths in the $k_x = 0$ plane; (c) 3D band dispersion of the $k_x = 0$ plane around point Γ. (d) Shapes of the Γ-centered NR of the $k_x = 0$ plane. The dotted and white solid lines in (c) and (d) represent the NR states in the $k_x = 0$ plane.

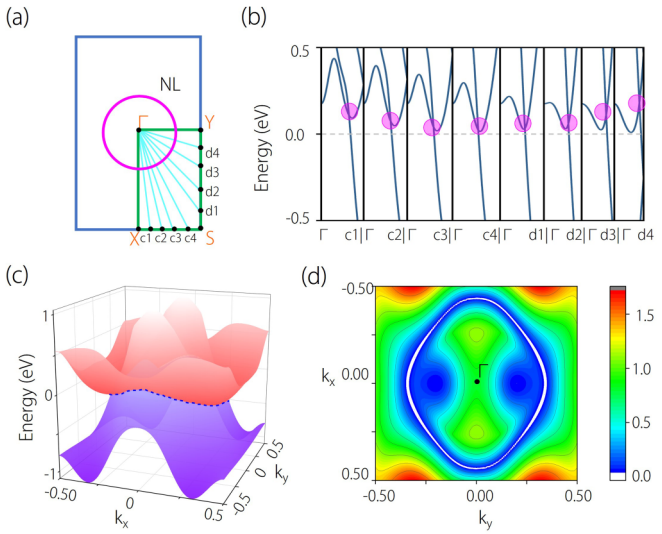

FIG. 4. (a) Selected k paths of the $k_z = 0$ plane, where the points c1–c4 (d1–d4) are equally spaced between X and S (S and Y); (b) band structures of the Γ-c1/c2/c3/c4 and Γ-d1/d2/d3/d4 paths in the $k_z = 0$ plane; (c) 3D band dispersion of the $k_z = 0$ plane around point Γ. (d) Shapes of the Γ-centered NR of the $k_z = 0$ plane. The dotted and white solid lines in (c) and (d) represent the NR states in the $k_z = 0$ plane.

The band structures along the abovementioned k paths are shown in Figs. 3(b), 4(b), and 5(b). The BCPs persist along all of the Γ-a1/a2/a3/a4, Γ-b1/b2/b3/b4, Γ-c1/c2/c3/c4 and Γ-d1/d2/d3/d4 paths, indicating that the closed NR states

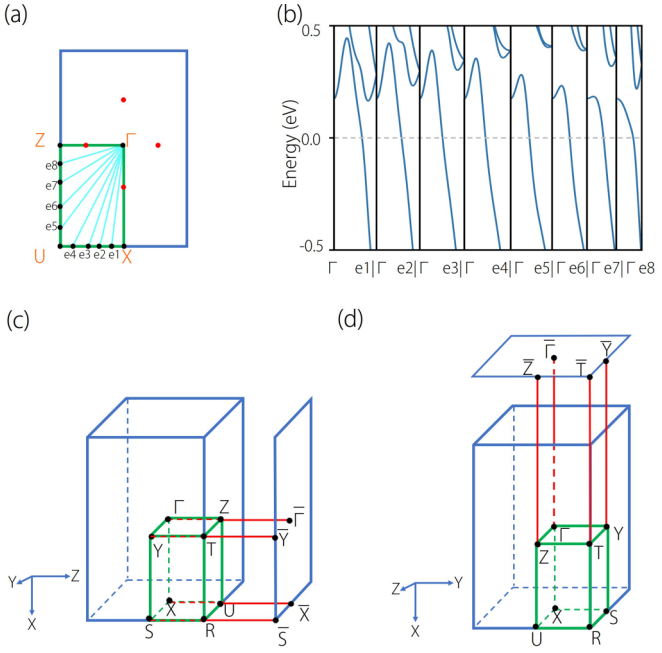

FIG. 5. (a) Selected k paths in the $k_y = 0$ plane, where the points e1–e4 (e5–e8) are equally spaced between X and U (U and Z); (b) band structures of the Γ-e1/e2/e3/e4 and Γ-e5/e6/e7/e8 paths in the $k_y = 0$ plane; (c) and (d) bulk BZ and surface BZ of the [001] surface and [100] surface, respectively.

exist in the $k_x = 0$ and $k_z = 0$ planes. In addition, we plot the 3D Γ-centered band structures and the shapes of the closed NRs of both planes in Figs. 3(c) and 4(c), and Figs. 3(d) and 4(d), respectively. However, in the band structures along the k paths, namely, Γ-e1/e2/e3/e4 and Γ-e5/e6/e7/e8, of the $k_y = 0$ plane, no BCPs occur [see Fig. 5(b)]. Moreover, the two NRs in the $k_x = 0$ and $k_z = 0$ planes share the same center point Γ, reflecting that FeB_4 is a TM with intersecting nodal rings (INRs) [44–47] in the momentum space [see Fig. 1(b)]. The INRs are extremely close to the E_F, and the energies of these two closed NRs vary within small ranges [see Figs. 3(b) and 4(b)].

To further discuss the INR states of this system, we attempt to understand them based on the effective Hamiltonian. The little group at point Γ belongs to the D_{2h} generated by $M_x : (x, y, z) \to (-x, y, z)$, $M_y : (x, y, z) \to (x + \frac{1}{2}, -y + \frac{1}{2}, z + \frac{1}{2})$ and $M_z : (x, y, z) \to (x + \frac{1}{2}, y + \frac{1}{2}, -z + \frac{1}{2})$. On plane $k_x = 0$, the D_{2h} point group has two 1D irreducible representations which could protect a nodal ring. The basis state of these two 1D representations can be chosen as $\{x,\ z\}$. In this basis, the generating elements of the group D_{2h} are therefore given by

$$M_x = -\sigma_z,\ M_y = \sigma_0,\ M_z = \sigma_z. \tag{1}$$

The effective Hamiltonian is required to be invariant under these three mirror symmetry transformations, such that

$$M_x \mathcal{H}(\boldsymbol{k}) M_x^{-1} = \mathcal{H}(-k_x, k_y, k_z), \tag{2}$$

$$M_y \mathcal{H}(\boldsymbol{k}) M_y^{-1} = \mathcal{H}(k_x, -k_y, k_z), \tag{3}$$

$$M_z \mathcal{H}(\boldsymbol{k}) M_z^{-1} = \mathcal{H}(k_x, k_y, -k_z). \tag{4}$$

For the off diagonal term, it must be the odd order of k_x or k_z due to $\{\sigma_z, \sigma_{x/y}\} = 0$. And mirrors $M_{x/z}$ also requires the diagonal term to be of k-quadratic dependence. Furthermore, the presence of $\mathcal{T}$ requires a real Hamiltonian. Consequently, the effective Hamiltonian is given as

$$\mathcal{H}(\boldsymbol{k}) = w(\boldsymbol{k})\sigma_0 + \left[M + Ak_x^2 + Bk_y^2 + Ck_z^2\right]\sigma_z + \gamma k_x k_z \sigma_x. \tag{5}$$

Here, $w(\boldsymbol{k})$ is the overall energy shift, and M, A, B, and C are real parameters.

In the same way, the effective Hamiltonian for the nodal ring on $k_z = 0$ takes the same form. Based on Eq. (5), it indicates that on plane $k_x = 0$ and $k_z = 0$, the off-diagonal term vanishes. The NRs on these two planes are determined by the diagonal term, which is proportional to σ_z. For example, with respect to the NR on $k_x = 0$ plane, we have the diagonal term $h_{k_x=0}(0, k_y, k_z) = M + Bk_y^2 + Ck_z^2 = 0$, where $MB < 0$ and $MC < 0$, which leads to a 1D band crossing between these two bands on this plane. The crossing bands are characterized by opposite eigenvalues of M_x, namely, $g_x = \pm 1$. It is stable as long as the M_x preserves. Referring to the NR on plane $k_z = 0$, the band crossing is determined by $h_{k_z=0}(k_x, k_y, 0) = M + Ak_x^2 + Bk_y^2 = 0$, also with $MB < 0$ and $MA < 0$, thus establishing a ring protected by M_z. Therefore, it is proved that there are two NRs, as shown in Fig. 1(b).

In addition to the BCPs P1, P2, and P3, in Fig. 2, two bands linearly cross at the Y and Z points (see the red arrows).

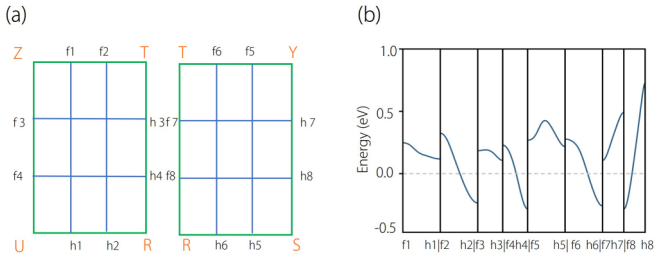

FIG. 6. (a) Selected k paths of the $k_y = \pi$ and $k_z = \pi$ planes and (b) band structures of the f1-h1/f2-h2/f3-h3/f4-h4/f5-h5/f6-h6/f7-h7/f8-h8 paths.

However, along the paths, S-Y/Z-U-R-T-Z/Y-T/S-R, the two bands degenerate, forming a nodal wall state, also called a nodal surface state [26–28,48,49]. We believe that the nodal walls should be appeared in the $k_y = \pi$ and $k_z = \pi$ planes. To further confirm the nodal walls of these two planes, we performed a detailed electronic-structures calculation based on the selected k paths in the $k_y = \pi$ and $k_z = \pi$ planes. The selected k paths are shown in Fig. 6(a), and the calculated band structures along the f1-h1/f2-h2/f3-h3/f4-h4/f5-h5/f6-h6/f7-h7/f8-h8 paths are shown in Fig. 6(b). From Fig. 6(b), one finds that all of the band structures are degenerated in both planes, indicating the presence of nodal wall states. Moreover, the nodal wall states are closed along the k_y and k_z directions [see Fig. 1(b)].

Notably, the closed nodal wall/surface states along the k_y and k_z directions are essential, and their formation can be analyzed in terms of symmetry. When SOC is not included, such surfaces are enforced by the combination of a twofold screw symmetry and $\mathcal{T}$. Indeed, there exist two screw rotations perpendicular to each other. The two screw rotations can be derived by combing two of these three mirrors, namely, $S_{2y} = M_x M_z$, $S_{2z} = M_x M_y$. Specifically, their operations in real space are obtained,

$$(x, y, z) \xrightarrow{S_{2y}} \left(-x + \tfrac{1}{2}, y + \tfrac{1}{2}, -z + \tfrac{1}{2}\right), \tag{6}$$

$$(x, y, z) \xrightarrow{S_{2z}} \left(-x + \tfrac{1}{2}, -y + \tfrac{1}{2}, z + \tfrac{1}{2}\right). \tag{7}$$

Accordingly, we have $(S_{2y})^2 = T_{010} = e^{-ik_y}$ and $(S_{2z})^2 = T_{001} = e^{-ik_z}$, where T_{010} and T_{001} are the translations along the y and z directions, respectively. Because $\mathcal{T}$ is an antiunitary operator and inverses the momentum $\boldsymbol{k}$, the combined operator $\mathcal{T}S_{2i}$ $(i = y, z)$ is antiunitary and only inverse the momentum along the i direction. Furthermore, $\mathcal{T}S_{2i}$ satisfies

$$(\mathcal{T}S_{2i})^2 = e^{-ik_i}, \tag{8}$$

such that the nodal surface can be understood from the Kramer degeneracy. On the corresponding planes $k_y = \pi$, $k_z = \pi$, we have

$$(\mathcal{T}S_{2y})^2 = -1, \tag{9}$$

$$(\mathcal{T}S_{2z})^2 = -1, \tag{10}$$

on the entire corresponding planes. Thus a double degenerate nodal wall/surface occurs [see Fig. 1(b)].

Before closing this section, note the following remarks. (1) Nodal surface semimetals with two-dimensional (2D) TE was firstly proposed by Zhong *et al.* and Liang *et al.* [50,51]. in 2016. In 2018, Wu *et al.* [27] discussed two classes of nodal surfaces in the absence of spin-orbit coupling (SOC). These two types are quite different, namely the class-I surfaces are topologically charged, however, the class-II ones are mainly originated from the topological features of screw symmetry. (2) Based on the arguments of Wu *et al.* [27], introducing SOC will generally destroy class-I nodal surfaces. However, if the inversion symmetry is broken and the SOC is added, $\mathcal{T}S_{2z}$-protected class-II nodal surfaces can be maintained in the $k_z = \pi$. Unfortunately, when SOC is considered, no realistic semimetals have been proposed to be class-II nodal surface semimetals to this date. (3) In many cases, $\mathcal{T}S_{2z}$ symmetry guarantees the nodal surface states on $k_z = \pi$ plane. If there are two or three $\mathcal{T}S_{2i}(i = x, y, z)$ symmetries at the same time, the system will have nodal surface states on multiple boundaries of the BZ. As shown in Fig. 1(b), our proposed nodal wall states belong to the multiple nodal surface states. Such multiple nodal surface states may bring some special physical properties. For example, Yu *et al.* [26] constructed a topological phase of a $\mathcal{T}$-invariant crystalline metal with multiple nodal surfaces covering the entire BZ boundary, and these multiple nodal surfaces can be used to circumvent the no-go theorem. Therefore, in the model proposed by Yu *et al.* [26], a single Weyl point is allowed to reside at the center of the BZ; (4)Although the nodal points and NLs with 0D and 1D band degeneracies have been confirmed in photonics and acoustics [52,53], the nodal wall, that is, the nodal surface state has not been observed in any classical-wave system before 2019. Yang *et al.* [54], for the first time, confirmed the nodal wall states in a 3D chiral acoustic crystal. Hence, it is hoped that the nodal wall state of FeB_4 can be experimentally confirmed soon.

IV. SURFACE STATES AND EFFECT OF SOC

For nodal line (NL) materials, we can observe the drum-head-like (D-H-L) surface states arising from the projected bulk NLs [55–59]. In this section, we calculate the projected spectrum of the FeB_4 [001] and [100] surface states along the $\bar{X}$-$\bar{\Gamma}$-$\bar{Y}$ and $\bar{Y}$-$\bar{\Gamma}$-$\bar{Z}$ surface BZ to confirm the appearance of the D-H-L surface states [see Figs. 7(b) and 7(d)]. For comparison, the band structures with marked BCPs along the X-Γ-Y and Y-Γ-Z 3D bulk paths are illustrated in Figs. 7(a) and 7(c). Figures 7(b) and 7(d) indicate the clear presence of D-H-L surface states on the [001] and [100] surfaces arising from the four BCPs in FeB_4. Hopefully, such clear surface states can be observed by using surface-sensitive detection methods.

We need to the study the effects of SOC on the electronic structures and BCPs of FeB_4. The calculated electronic structures of band structures of FeB_4 under the SOC effect are shown in Fig. 8. The opened gaps for the NR and nodal wall states are smaller than 39 meV. The values of the SOC-induced gaps in FeB_4 are comparable to those in the experimentally confirmed NL material Mg_3Bi_2 (> 36 meV) [60,61], and they are smaller than those of a few well-known topological materials (with SOC-induced gaps larger

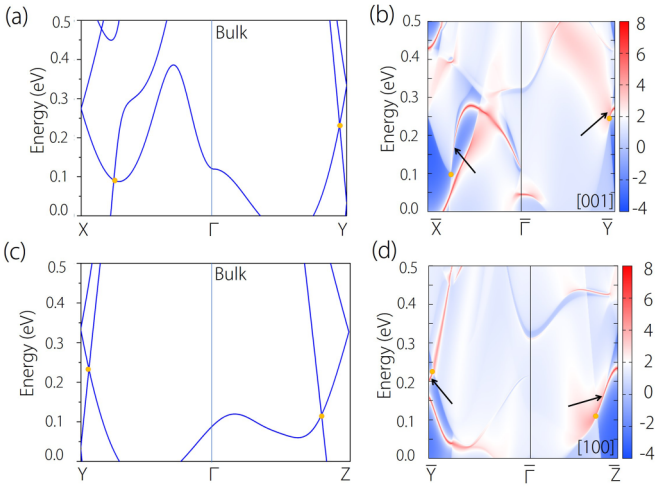

FIG. 7. [(a) and (c)] Band structures of bulk FeB_4 along the X-Γ-Y and Y-Γ-Z paths, respectively. [(b) and (b)] [001] and [100] surface states of FeB_4 along the surface BZ $\bar{X}$-$\bar{\Gamma}$-$\bar{Y}$ and $\bar{Y}$-$\bar{\Gamma}$-$\bar{Z}$, respectively. The positions of the BCPs are marked by yellow dots, and the drum-head-like surface states arising from the BCPs are marked by black arrows.

than 40 meV), such as CaTe (50–52 meV) [62], Zn_3Bi_2 (∼65.9 meV) [63], Hg_3Bi_2 (∼100.2 meV) [63], Cu_3PdN (> 60 meV) [64], $CaAs_3$ (39.92–54.47 meV) [42] and CaAgBi (> 80 meV) [65].

Before closing this section, note that the symmetry protected nodal lines can also be found in some materials with strong SOC [66]. As an example, Sun [67] predicted the robust bulk nodal lines and topological surface states with SOC in $PbTaS_2$ in 2017. In 2020, Gao *et al*. [68] reported that $PbTaS_2$ is also a weakly coupled type-II superconductor with transition temperature T_c (about 2.6 K) in the experiment.

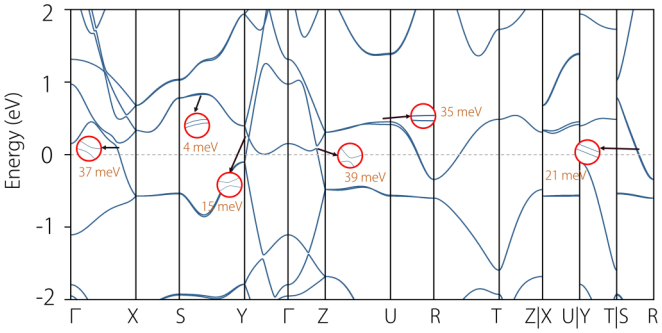

FIG. 8. The calculated band structure of FeB_4. SOC is considered.

V. CONCLUSION

In this work, we investigated the topological elements in superhard FeB_4 superconductor. This system exhibits INR states (centered at point Γ) in the $k_x = 0$ and $k_z = 0$ planes and closed nodal walls (along the k_y and k_z directions) in the $k_y = \pi$ and $k_z = \pi$ planes. Based on the obtained band structures under the SOC effect, we can conclude that the SOC-induced gaps in these topological signatures of FeB_4 are comparable to those of an experimentally confirmed NL material Mg_3Bi_2. Clear D-H-L surface states were found on the [100] and [001] surfaces, reflecting the 1D NR states of the FeB_4 bulk material. Our study revealed that FeB_4 with the *Pnnm* structure could serve as a novel single-phase topological superconductor material.

ACKNOWLEDGMENTS

X.T.W. is grateful for the support from the National Natural Science Foundation of China (No. 51801163) and the Natural Science Foundation of Chongqing (No. cstc2018jcyjA0765). Y.L. is grateful for the support from the Nature Science Foundation of Hebei Province (No. A2021202002).

[1] M. Sato and Y. Ando, Rep. Prog. Phys. **80**, 076501 (2017).
[2] L. Fu and E. Berg, Phys. Rev. Lett. **105**, 097001 (2010).
[3] F. Zhang, C. L. Kane, and E. J. Mele, Phys. Rev. Lett. **111**, 056402 (2013).
[4] C. Xu and L. Balents, Phys. Rev. Lett. **121**, 087001 (2018).
[5] A. C. Potter and P. A. Lee, Phys. Rev. B **85**, 094516 (2012).
[6] M. X. Wang, C. H. Liu, J. P. Xu, F. Yang, L. Miao, M. Y. Yao, C. L. Gao, C. Shen, X. Ma, X. Chen, Z. A. Xu, Y. Liu, S. C. Zhang, D. Qian, J. F. Jia, and Q. K. Xue, Science **336**, 52 (2012).
[7] L. Zhao, H. Deng, I. Korzhovska, M. Begliarbekov, Z. Chen, E. Andrade, E. Rosenthal, A. Pasupathy, V. Oganesyan, and L. K. Elbaum, Nat. Commun. **6**, 8279 (2015).
[8] M. Meinert, Phys. Rev. Lett. **116**, 137001 (2016).
[9] P. J. Guo, H. C. Yang, K. Liu, and Z. Y. Lu, Phys. Rev. B **95**, 155112 (2017).
[10] X. H. Tu, P. F. Liu, and B. T. Wang, Phys. Rev. Mater. **3**, 054202 (2019).
[11] H. Tang, D. Liang, R. J. Qiu, and S. P. A. Gao, ACS Nano **5**, 7510 (2011).
[12] Y. S. Hor, A. J. Williams, J. G. Checkelsky, P. Roushan, J. Seo, Q. Xu, H. W. Zandbergen, A. Yazdani, N. P. Ong, and R. J. Cava, Phys. Rev. Lett. **104**, 057001 (2010).
[13] Z. Liu, X. Yao, J. Shao, M. Zuo, L. Pi, S. Tan, C. Zhang, and Y. Zhang, J. Am. Chem. Soc. **137**, 10512 (2015).
[14] L. He, Y. Jia, S. Zhang, X. Hong, C. Jin, and S. Li, Npj Quant. Mater. **1**, 16014 (2016).
[15] X. C. Pan, X. Chen, H. Liu, Y. Feng, Z. Wei, Y. Zhou, Z. Chi, L. Pi, F. Yen, F. Song, X. Wan, Z. Yang, B. Wang, G. Wang, and Y. Zhang, Nat. Commun. **6**, 7805 (2015).
[16] Y. Qi, P. G. Naumov, M. N. Ali, C. R. Rajamathi, W. Schnelle, O. Barkalov, M. Hanand, S. C. Wu, C. Shekhar, Y. Sun, V. Süß, M. Schmidt, U. Schwarz, E. Pippel, P. Werner, R. Hillebrand, T. Forster, E. Kampert, S. Parkin, R. J. Cava *et al.*, Nat. Commun. **7**, 11038 (2016).
[17] B. Song, Y. Zhou, H. M. Yang, J. H. Liao, L. M. Yang, X. B. Yang, and E. Ganz, J. Am. Chem. Soc. **141**, 3630 (2019).
[18] L. Jin, X. Zhang, T. He, W. Meng, X. Dai, and G. Liu, J. Mater. Chem. C **7**, 10694 (2019).

[19] X. Zhang, Z. M. Yu, X. L. Sheng, H. Y. Yang, and S. A. Yang, Phys. Rev. B **95**, 235116 (2017).

[20] K. H. Jin, H. Huang, J. W. Mei, Z. Liu, L. K. Lim, and F. Liu, Npj Comput. Mater. **5**, 57 (2019).

[21] G. Bian, T. R. Chang, R. Sankar, S. Y. Xu, H. Zheng, T. Neupert, C. K. Chiu, S. M. Huang, G. Chang, I. Belopolski, D. S. Sanchez, M. Neupane, N. Alidoust, C. Liu, B. Wang, C. C. Lee, H. T. Jeng, C. Zhang, Z. Yuan, S. Jia *et al.*, Nat. Commun. **7**, 10556 (2016).

[22] D. Y. Chen, Y. Wu, L. Jin, Y. K. Li, X. X. Wang, J. X. Duan, J. F. Han, X. Li, Y. Z. Long, X. M. Zhang, D. Chen, and B. Teng, Phys. Rev. B **100**, 064516 (2019).

[23] E. Cheng, W. Xia, X. Shi, Z. Yu, L. Wang, L. Yan, D. C. Peets, C. Zhu, H. Su, Y. Zhang, D. Dai, X. Wang, Z. Zou, N. Yu, X. Kou, W. Yang, W. Zhao, Y. Guo, and S. Li, Npj Quant. Mater. **5**, 38 (2020).

[24] M. Qi, X. Zhu, Y. Zhou, C. An, C. Chen, Y. Yuan, and R. Zhang, Adv. Electron. Mater. **6**, 2000293 (2020).

[25] Y. Li, Z. Wu, J. Zhou, K. Bu, C. Xu, L. Qiao, M. Li, H. Bai, J. Ma, Q. Tao, C. Cao, Y. Yin, and Z. A. Xu, Phys. Rev. B **102**, 224503 (2020).

[26] Z. M. Yu, W. Wu, Y. X. Zhao, and S. A. Yang, Phys. Rev. B **100**, 041118(R) (2019).

[27] W. Wu, Y. Liu, S. Li, C. Zhong, Z. M. Yu, X. L. Sheng, Y. X. Zhao, and S. A. Yang, Phys. Rev. B **97**, 115125 (2018).

[28] X. Zhang, Z. M. Yu, Z. Zhu, W. Wu, S. S. Wang, X. L. Sheng, and S. A. Yang, Phys. Rev. B **97**, 235150 (2018).

[29] H. Gou, N. Dubrovinskaia, E. Bykova, A. A. Tsirlin, D. Kasinathan, W. Schnelle, A. Richter, M Merlini, M. Hanfland, A. M. Abakumov, D. Batuk, G. VanTendeloo, Y. Nakajima, A. N. Kolmogorov, and L. Dubrovinsky, Phys. Rev. Lett. **111**, 157002 (2013).

[30] G. Kresse and J. Furthmuller, Phys. Rev. B **54**, 11169 (1996).

[31] J. P. Perdew, K. Burke, and M. Ernzerhof, Phys. Rev. Lett. **77**, 3865 (1996).

[32] J. P. Perdew, K. Burke, and M. Ernzerhof, Phys. Rev. Lett. **80**, 891 (1998).

[33] Q. Wu, S. Zhang, H. Song, M. Troyer, and A. Soluyanov, Comput. Phys. Commun. **224**, 405 (2018).

[34] J. Taylor, H. Guo, and J. Wang, Phys. Rev. B **63**, 245407 (2001).

[35] M. Onoda and N. Nagaosa, J. Phys. Soc. Jpn. **71**, 19 (2002).

[36] K. H. Kim, B. J. Yang, and H. W. Lee, Phys. Rev. B **98**, 245422 (2018).

[37] B. Dorado, B. Amadon, M. Freyss, and M. Bertolus, Phys. Rev. B **79**, 235125 (2009).

[38] C. Loschen, J. Carrasco, K. M. Neyman, and F. Illas, Phys. Rev. B **75**, 035115 (2007).

[39] See Supplemental Material at http://link.aps.org/supplemental/10.1103/PhysRevMaterials.5.074201 for calculated band structure of FeB_4 with GGA + U methods.

[40] H. Weng, Y. Liang, Q. Xu, R. Yu, Z. Fang, X. Dai, and Y. Kawazoe, Phys. Rev. B **92**, 045108 (2015).

[41] C. Fang, H. Weng, X. Dai, and Z. Fang, Chin. Phys. B **25**, 117106 (2016).

[42] Q. Xu, R. Yu, Z. Fang, X. Dai, and H. Weng, Phys. Rev. B **95**, 045136 (2017).

[43] R. Yu, Z. Fang, X. Dai, and H. Weng, Front. Phys. **12**, 127202 (2017).

[44] C. Gong, Y. Xie, Y. Chen, H. S. Kim, and D. Vanderbilt, Phys. Rev. Lett. **120**, 106403 (2018).

[45] X. Wang, G. Ding, Z. Cheng, X. L. Wang, G. Zhang, and T. Yang, J. Mater. Chem. C **8**, 5461 (2020).

[46] Y. J. Jin, Z. J. Chen, B. W. Xia, Y. J. Zhao, R. Wang, and H. Xu, Phys. Rev. B **98**, 220103(R) (2018).

[47] J. Cai, Y. Xie, P. Chang, H. Kim, and Y. Chen, Phys. Chem. Chem. Phys. **20**, 21177 (2018).

[48] Y. Qie, J. Liu, S. Wang, Q. Sun, and P. Jena, J. Mater. Chem. A **7**, 5733 (2019).

[49] T. Yang and X. Zhang, J. Mater. Chem. C **8**, 9046 (2020).

[50] C. Zhong, Y. Chen, Y. Xie, S. A. Yang, M. L. Cohen, and S. B. Zhang, Nanoscale **8**, 7232 (2016).

[51] Q. F. Liang, J. Zhou, R. Yu, Z. Wang, and H. Weng, Phys. Rev. B **93**, 085427 (2016).

[52] L. Lu, J. D. Joannopoulos, and M. Soljčić, Nat. Photonics **8**, 821 (2014).

[53] Z. Yang, F. Gao, X. Shi, X. Lin, Z. Gao, Y. Chong, and B. Zhang, Phys. Rev. Lett. **114**, 114301 (2015).

[54] Y. Yang, J. Xia, H. Sun, Y. Ge, D. Jia, S. Yuan, and B. Zhang, Nat. Commun. **10**, 2521 (2019).

[55] H. Zhang, X. Zhang, T. He, X. Dai, Y. Liu, G. Liu, L. Wang, and Y. Zhang, Phys. Rev. B **102**, 155116 (2020).

[56] C. Chen, Z. M. Yu, S. Li, Z. Chen, X. L. Sheng, and S. A. Yang, Phys. Rev. B **99**, 075131 (2019).

[57] S. Li, Y. Liu, S. S. Wang, Z. M. Yu, S. Guan, X. L. Sheng, Y. G. Yao, and S. A. Yang, Phys. Rev. B **97**, 045131 (2018).

[58] S. Li, Y. Liu, B. Fu, Z. M. Yu, S. A. Yang, and Y. Yao, Phys. Rev. B **97**, 245148 (2018).

[59] G. Liu, L. Jin, X. Dai, G. Chen, and X. Zhang, Phys. Rev. B **98**, 075157 (2018).

[60] X. Zhang, L. Jin, X. Dai, and G. Liu, J. Phys. Chem. Lett. **8**, 4814 (2017).

[61] T. R. Chang, I. Pletikosic, T. Kong, G. Bian, A. Huang, J. Denlinger, and W. Xie, Adv. Sci. **6**, 1800897 (2019).

[62] Y. Du, F. Tang, D. Wang, L. Sheng, E. J. Kan, C. G. Duan, and X. Wan, Npj Quant. Mater. **2**, 3 (2017).

[63] J. L. Lu, W. Luo, X. Y. Li, S. Q. Yang, J. X. Cao, X. G. Gong, and H. J. Xiang, Chin. Phys. Lett. **34**, 057302 (2017).

[64] Y. Kim, B. J. Wieder, C. L. Kane, and A. M. Rappe, Phys. Rev. Lett. **115**, 036806 (2015).

[65] F. Tran and P. Blaha, Phys. Rev. Lett. **102**, 226401 (2009).

[66] C. Fang, Y. Chen, H.-Y. Kee, and L. Fu, Phys. Rev. B **92**, 081201(R) (2015).

[67] J.-P. Sun, Chin. Phys. Lett. **34**, 077101 (2017).

[68] J. J. Gao, J. G. Si, X. Luo, J. Yan, Z. Z. Jiang, W. Wang, C. Q. Xu, X. F. Xu, P. Tong, W. H. Song, X. B. Zhu, W. J. Lu, and Y. P. Sun, J. Phys. Chem. C **124**, 6349 (2020).